Geophysical Research Letters

RESEARCH LETTER
10.1029/2021GL096126

Key Points:

- Dynamical core model is overly predictable vis-à-vis the comprehensive model
- Reduced Eady growth rates are associated with a longer time to error saturation
- Midlatitude error growth in the comprehensive model is quicker in warmer climates and slower in cooler climates

Supporting Information:

Supporting Information may be found in the online version of this article.

Correspondence to:

A. Sheshadri,
Aditi_Sheshadri@stanford.edu

Citation:

Sheshadri, A., Borrus, M., Yoder, M., & Robinson, T. (2021). Midlatitude error growth in atmospheric GCMs: The role of eddy growth rate. *Geophysical Research Letters*, *48*, e2021GL096126. https://doi.org/10.1029/2021GL096126

Received 21 SEP 2021
Accepted 19 NOV 2021

Midlatitude Error Growth in Atmospheric GCMs: The Role of Eddy Growth Rate

Aditi Sheshadri[1], Marshall Borrus[1], Mark Yoder[1], and Thomas Robinson[2,3]

[1]Department of Earth System Science, Stanford University, Palo Alto, CA, USA, [2]Geophysical Fluid Dynamics Laboratory, Princeton, NJ, USA, [3]SAIC, Princeton, NJ, USA

Abstract Several studies have established that atmospheric flows have a finite range of predictability, which may be reasonably considered a consequence of the underlying dynamics. In the midlatitudes, error growth is predominantly associated with baroclinic disturbances. We consider midlatitude error growth in two models: an idealized dry dynamical core and a comprehensive atmospheric general circulation model (GCM). By systematically varying equator to pole temperature gradients in the dynamical core, we show that with increasing Eady growth rates, the time elapsed before errors saturate decreases, shortening the window in which weather predictions may be useful. We also consider the limits of midlatitude predictability in the comprehensive moist GCM in a range of climates. Our results show that the times to error saturation are shorter in warmer climates than colder climates, suggesting that warmer climates are inherently less predictable.

Plain Language Summary It is well understood that weather predictions are only useful for a limited period. In the middle latitudes of the Earth, flows in the atmosphere are set by the effects of midlatitude storms. Understanding factors that set the limit up to which weather predictions are useful may help us improve our ability to provide accurate forecasts and prepare for changes in the period of useful weather prediction in different climates. We show in this work that the time scale over which eddies grow can change the time that models take to lose memory of initial conditions, thus changing the period over which weather predictions may be useful. Many realizations of a comprehensive atmospheric model run in a range of cold to warm conditions also reveal that midlatitude weather may be less predictable in warmer climates than colder climates.

1. Introduction

Lorenz (1969) first suggested that atmospheric flows might have a finite range of predictability. The chaotic divergence of model trajectories due to small errors in initial conditions is now widely accepted, following numerous studies involving atmospheric models of differing complexity (e.g., Daley, 1981; Sun & Zhang, 2016 and many others). In the case of midlatitude weather systems, several studies (e.g., Froude et al., 2013; Smagorinsky, 1969) estimate this finite range to be about two weeks. Thus, weather forecasts are only useful up to this intrinsic range (e.g., Palmer et al., 2014). Gaining an understanding of the factors that set this time scale may enable an informed expectation of its value in altered climates and lead to improvements in numerical weather prediction.

Error growth and thus predictability in different latitude ranges may be reasonably considered a consequence of the underlying dynamics, with the flow (and thus error propagation) in the middle latitudes predominantly associated with baroclinic disturbances (e.g., Judt, 2020). Additionally, the properties of error growth may be different in models at varying levels of complexity.

In this work, we consider midlatitude error growth in two models: an idealized dry dynamical core and a comprehensive atmospheric GCM. The model setups we consider are described in Section 2. Section 3 relates error propagation with midlatitude eddies simulated by these models, using the Eady growth rate as an indicator of the time scales of growth of baroclinic eddies. Section 4 focuses on predictability in altered climates in the comprehensive model, including the effects of altered moisture content on static stability.

2. Model Setup

2.1. Dry Dynamical Core Integrations

The dry dynamical core model is based on that of Polvani and Kushner (2002), and is identical to that of Sheshadri and Plumb (2016). The model is dry and hydrostatic, solving the global primitive equations with T42 resolution in the horizontal and 40 sigma levels in the vertical. Radiation and convection schemes are replaced by relaxation to a zonally symmetric equilibrium temperature profile identical to Held and Suarez (1994) in the troposphere. In the stratosphere (above 200 hPa), the equilibrium temperature profile is specified, incorporating the seasonal cycle of Sheshadri et al. (2015). An ensemble of 400-day integrations is generated by setting the value of the *initial_perturbation* (a vorticity perturbation that is added to the initial conditions in the Held and Suarez (1994) model to initiate baroclinic instability) to linearly step between values of 1.0e−7 and 2.0e−7 to generate 20 branch integrations. Further ensembles of three integrations each with altered equator to pole temperature gradients are run. The tropospheric equator to pole temperature gradient in the equilibrium temperature specifications [the parameter δy in Equation A4 from Polvani and Kushner (2002)] is varied between 10 and 70 K, with the default being 60 K.

2.2. AM4 Integrations

The comprehensive model data in our study were generated using the Geophysical Fluid Dynamics Laboratory (GFDL) Atmosphere Model 4.0 (AM4.0; Zhao et al., 2018a, 2018b). AM4.0 was developed at GFDL and used as part of Coupled Model Intercomparison Project Phase 6 (CMIP6; Eyring et al., 2016). The base run setup uses the default input data and parameters as shared by GFDL (https://github.com/NOAA-GFDL/AM4), with small perturbations to initial conditions introduced through a namelist variable "*add_noise*." The model is run with specified sea surface temperature (SST), with seasonally varying insolation and a sea-ice distribution as described in Zhao et al. (2018a). In all other setups, we vary SST as either a uniform or zonally symmetric forcing.

AM4.0 uses the GFDL Finite-Volume Cubed-Sphere Dynamical Core (FV^3) (Harris & Lin, 2013; Putman & Lin, 2007) with 96×96 grid boxes per cube face. Each model run was integrated for 100 days, with a horizontal grid spacing of approximately 100 km (C96) and 33 levels in the vertical. The model top is at 1 hPa. Horizontal winds, temperature, and precipitation were recorded at daily intervals. To reduce computational complexity, the processes related to oceans are turned off for all our integrations, keeping the related initial conditions static through the run. In all integrations, we introduce 0.0333 K of random thermal noise during initialization to seed errors between integrations of the same parameters and initial conditions. Model runs were conducted on Sherlock, a High-Performance Computing (HPC) cluster, operated by the Stanford Research Computing Center.

A total of 17 model setups were analyzed, each with a different SST profile. Details of AM4 integrations are summarized in Table S1 in Supporting Information S1, and the corresponding SST profiles are shown in Figure S1 in Supporting Information S1. The base model setup uses the default prescribed SST profile (Figure S1 in Supporting Information S1) and consists of 20 integrations. Eight setups used SST profiles uniformly adjusted in increments of 1°C from −4 to +4 °C. The first and last setups in this range consist of 20 integrations each, and the six intermediary configurations consist of two integrations each.

Eight setups use Qobs SST profiles defined by Neale and Hoskins (2000). The Qobs SST distribution is zonally symmetric, peaking at the equator, and decreasing geometrically to zero at 60N and 60S. In our perturbation runs, we scale this Qobs profile by factors that range from −16 to 16 in increments of 4K. The Qobs distributions change the equator to pole temperature gradient whereas the uniform adjustments do not. The +4 and −4 °C configurations consist of four integrations each, and the ±8, ±12, and ±16 °C configurations consist of three integrations each. While forced warming only occurs in the sea surface, temperatures over land increase in step with temperatures above the ocean and become smoothly distributed in fewer than 10 days.

3. Error Growth in the Dynamical Core

Figure 1 shows the growth of error in zonal wind and temperature averaged across all longitudes between 850-500 hPa, which we designate the lower troposphere, and 500-200 hPa, which we designate the upper troposphere, at 45°N. We focus here on 45°N, but other choices of midlatitudes in both hemispheres show similar results. Four

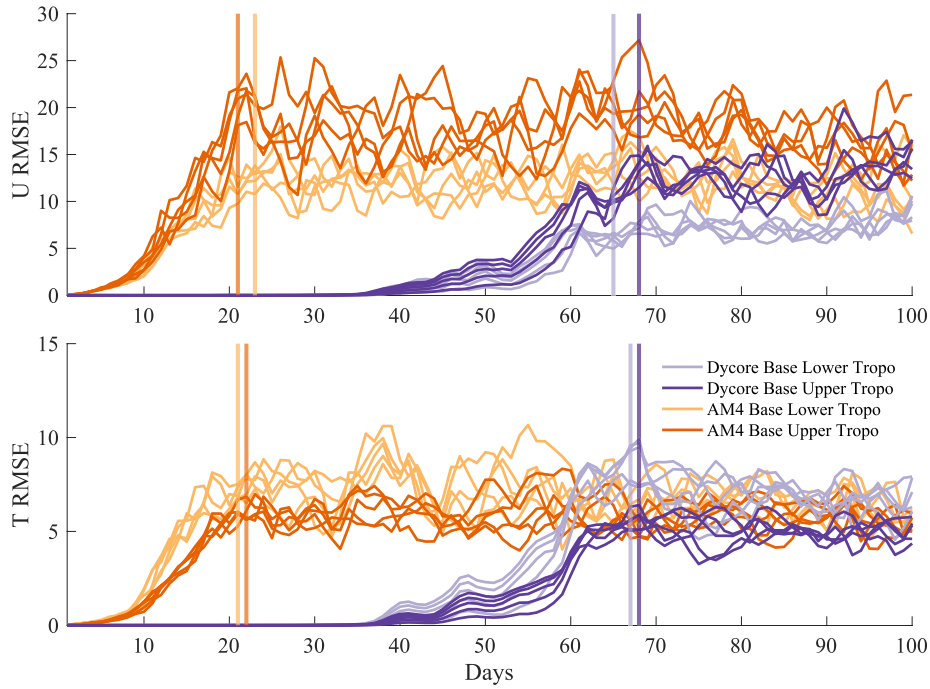

Figure 1. Root mean squared error in (top panel) zonal wind and (bottom panel) temperature for the base state (denoted h0) dynamical core integrations in purple and AM4 in orange for the upper and lower troposphere, averaged across longitudes at 45°N. The time to error saturation is marked with a vertical line.

of the integrations are shown for the control run of both model configurations for figure clarity. In both models, as the model branch integrations diverge from each other, error grows with time, and ultimately saturates (in agreement with previous studies, e.g., Krishnamurthy, 1993; Liu et al., 2009). Our method to identify saturation times is described in Supplement T1. It is evident that error growth in the dynamical core model is much slower than that in AM4, with saturation occurring at about 65–70 days as compared to 20–25 days in the AM4 integrations. The error in temperature at saturation is similar across the two models, but the saturated error in zonal wind is higher in AM4 (about 20 m/s versus 10 m/s in the upper troposphere in the dynamical core).

Since baroclinic instability is the likely facilitator of error growth in the midlatitudes, we calculate Eady growth rates (EGR) as an indicator of the time scales involved in the growth of baroclinic disturbances, and therefore of error. The EGR values are calculated as $\sigma = \left|\frac{f_o}{N}\frac{\partial \bar{u}}{\partial z}\right|$, where f_o is the Coriolis parameter, the static stability (buoyancy frequency) N is calculated as $N = \sqrt{\frac{g}{\theta}\frac{\partial \theta}{\partial z}}$, z is altitude, θ is potential temperature, and $\bar{u}$ is zonal mean zonal wind. Table 1 shows EGR calculated for the dynamical core and for AM4 output between 850 and 200 hPa, averaged between 42.5°N and 47.5°N. The differences in EGR between the base runs of the dynamical core and AM4 stem from differences in their static stability and vertical shear. In the case of AM4, we also estimate a moist Eady growth rate based on replacing the dry static stability with the effective static stability calculation of O'Gorman (2011), which represents a way of accounting for the effects on moisture on static stability and is a small correction to the dry growth rate.

To test the hypothesis that the basic state influences the time scales involved in the growth of errors (and hence the inherent predictability of these models), we consider a series of additional dynamical core simulations with altered equator to pole temperature gradients; error growth in zonal wind from these integrations is shown in Figure 2; error in other variables behaves similarly. Theories by Stone (1978) and Held (1982) relate the static stability with meridional temperature gradients, and more recently Frierson et al. (2006) and others have related moist stability to surface equivalent potential temperature gradients. In this idealized model, varying the parameter δy (see Equation A4 in Polvani and Kushner (2002); the parameter is also referred to as $(\Delta T)_y$ in Held and Suarez (1994)) is a trivial way to systematically alter the equator to pole temperature gradient, and thus static stability. As δy is varied between 10 and 70 K, the static stability and the vertical shear of the midlatitude

Table 1
Dry and Moist Eady Growth Rates, and Dry and Effective Stratification, and Vertical Shear at 45°N for the Dynamical Core and AM4 Integrations

	Run type	Dry EGR (1/days)	Moist EGR (1/days)	Dry N (1/days)	Moist N (1/days)	du/dz (1/days)
AM4 (Qobs)	−16°C	1.41	1.62	1,171	1,077	166
	−12°C	1.41	1.63	1,171	1,074	167
	−8°C	1.35	1.56	1,169	1,067	163
	−4°C	1.50	1.74	1,171	1,064	179
	Base	1.60	1.85	1,179	1,063	198
	+4°C	1.73	2.01	1,196	1,064	225
	+8°C	1.92	2.24	1,225	1,076	261
	+12°C	2.07	2.47	1,237	1,062	285
	+16°C	1.94	2.32	1,275	1,079	275
Dycore	10	0.1621	—	1,256	—	7
	20	0.3001	—	1,284	—	21
	30	0.3888	—	1,310	—	32
	40	0.4512	—	1,342	—	40
	50	0.4978	—	1,366	—	40
	60	0.5626	—	1,404	—	46
	70	0.665	—	1,427	—	40

atmosphere both increase, and baroclinic eddies grow more quickly (using the Eady growth rate as a measure) the time required for error to saturate (and thus, for the model to "forget" initial conditions) monotonically reduces.

4. Error Growth in a Range of AM4 Climates

To consider the question of predictability windows in a range of climates, we turn to the results from the comprehensive moist model integrations, which span a wide range of global mean surface temperature. Figure 3 shows error growth in terms of RMS errors in zonal wind and temperature for a selection of the AM4 integrations ranging from the coolest to the warmest climates. A clear trend emerges—the time to error saturation systematically reduces with warming. Thus, the comprehensive climate model takes longer to lose its "memory" of initial

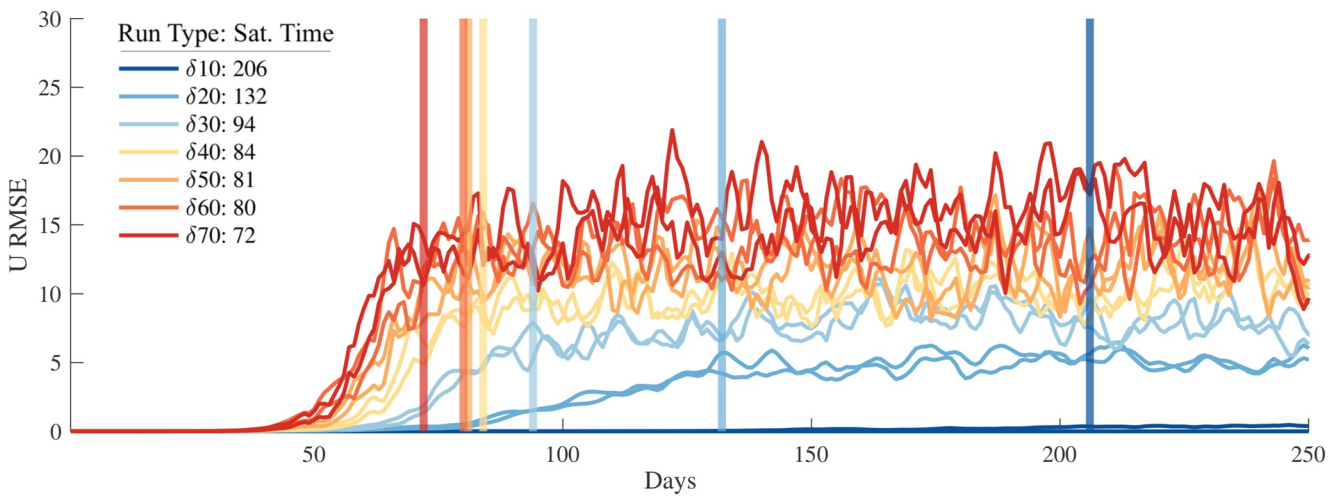

Figure 2. Root mean squared error in zonal wind across the dynamical core integrations, from $\delta y = 0$ in dark blue to $\delta y = 70$ in red. The time to error saturation is marked with a vertical line with the days to saturation listed next to the run names in the legend.

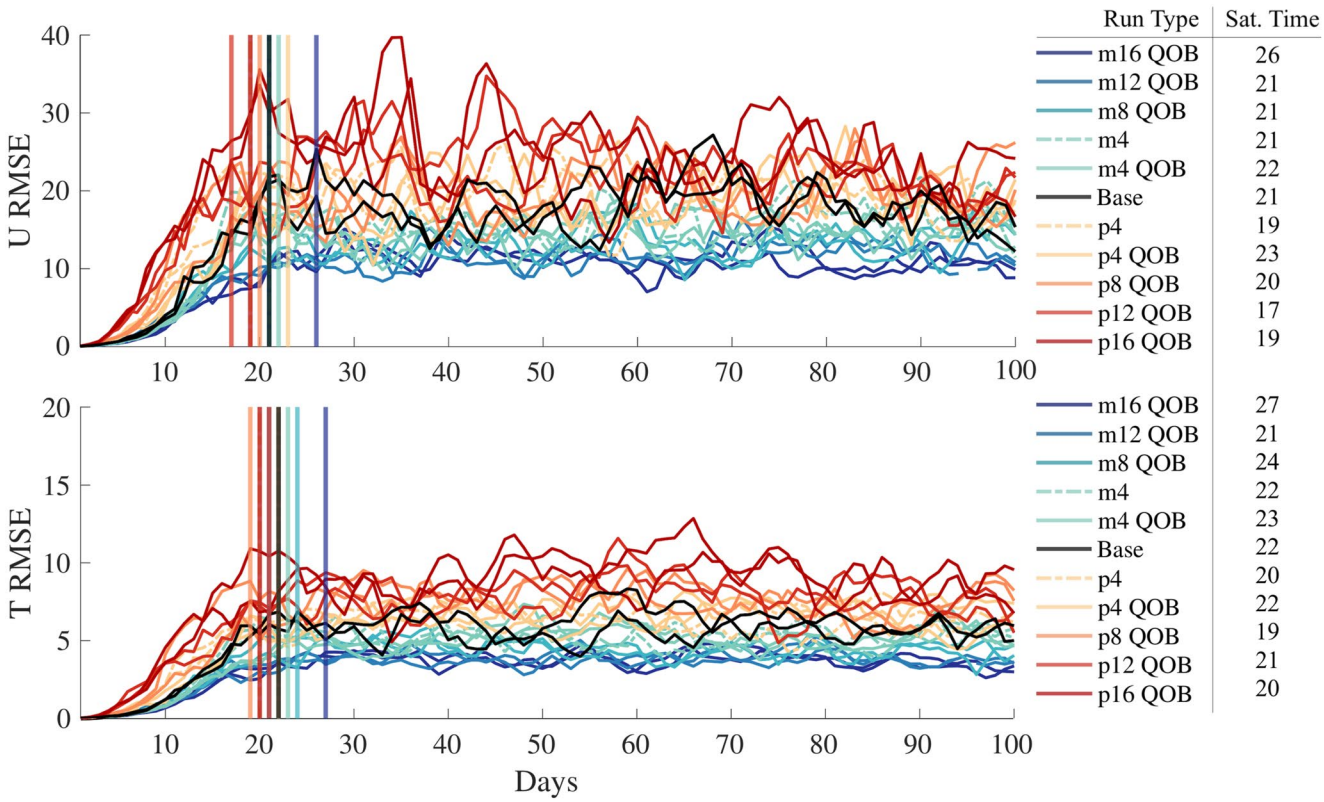

Figure 3. Root mean squared error in (top panel) zonal wind and (bottom panel) temperature for the various AM4 integrations, going from the coolest (dark shades of blue) to the warmest (dark shades of red) climates averaged across longitudes at 45°N. The time to error saturation is marked with a vertical line and listed in the legend.

conditions in cooler climates than warmer ones, indicating a reduction of predictability with warming. This holds across both the climates with uniform warming/cooling at all latitudes and in those that were perturbed with respect to the Qobs profile.

The latitudinal structure of EGR for these integrations are shown in Figure 4; these are consistent with the picture of increased static stability and vertical shear with warming leading to faster growth of eddies, and thus a reduction of the time to error saturation. Figure S2 in Supporting Information S1 shows changes in static stability as well as effective static stability between the simulations of a substantially cooler versus a substantially warmer planet, with SSTs set to Qobs ± 4°C. Figure 3 would suggest that the intrinsic limit on midlatitude weather predictability would vary between 17 and 28 days for the warmest and the coldest integration. In addition to the

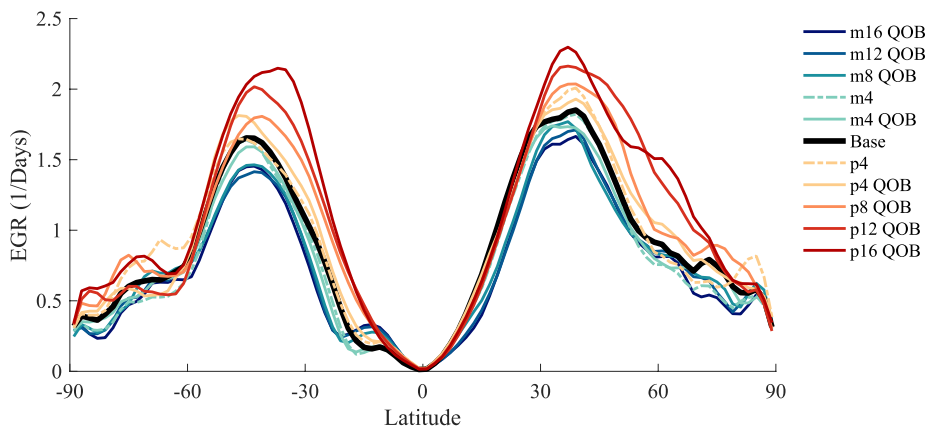

Figure 4. Eady growth rates for the same integrations as in Figure 3, averaged across the first 20 days of integration.

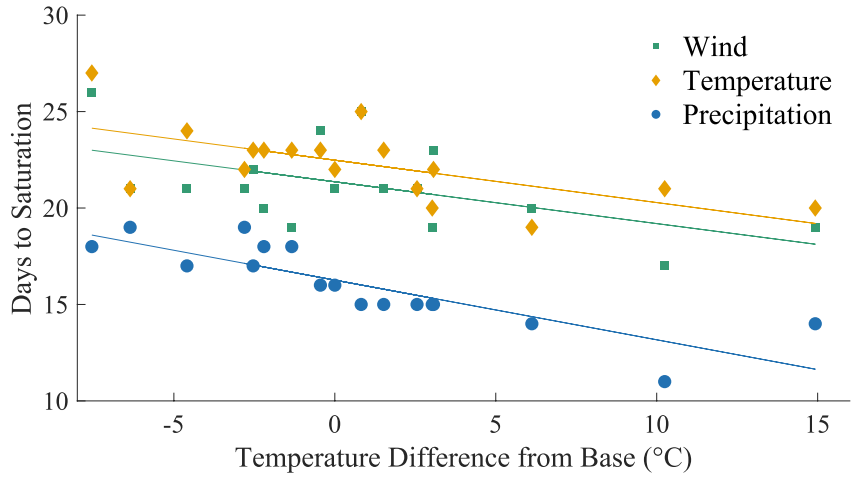

Figure 5. Time to error saturation for (green) zonal wind, (yellow) temperature, and (blue) precipitation across the AM4 simulations. The *x* axis shows column integrated temperature differences from a base integration (similar to present-day) at 45°N.

increased dry static stability under warming, the increased moisture content of a warmer atmosphere further modulates these effects through latent heat release (Figure S2 in Supporting Information S1 also shows the ratios of dry and effective static stability in the p4 and m4 integrations following the calculations of O'Gorman (2011) to provide representative numbers for a warm and a cold climate). We also note that additional complexities associated with AM4 vis-à-vis the dynamical core (e.g., the effects of sea ice, interactive radiation, higher horizontal resolution, better resolved teleconnections, etc.) may play roles in setting the rate of error growth in this comprehensive model.

5. Discussion and Conclusions

Understanding the factors that control inherent limits on atmospheric predictability, both in the current climate and those of the past and future, is of fundamental importance. In the midlatitudes, where the growth of error is set by baroclinic disturbances, we have shown that the model's basic state plays a key role in setting how quickly atmospheric models lose track of initial conditions.

In the comprehensive GCM, we have carried out a series of experiments in both colder and warmer conditions than present-day by modifying SSTs. From these we conclude that the time scales up to which predictions of midlatitude weather may be reliable decrease with increasing temperature. Figure 5 illustrates this, showing the time to error saturation in zonal wind, temperature, and precipitation as temperature changes, relative to conditions similar to the present observed atmosphere. We suggest that these changes could be attributed to increased static stability and vertical shear in zonal wind with warming, modified by the moisture content of the atmosphere. These results imply that under warming (cooling), the inherent predictability of the midlatitude atmosphere will reduce (increase). Initial analysis of the limited output that is available from the CMIP6 archive suggests that the EGR is indeed expected to increase toward the end of the century under the SSP245 scenario in CESM2-WACCM, but this calculation was performed using only two model levels that were available. There is also some suggestion that Arctic Sea ice loss has been associated with an increase in EGR (Simmonds & Li, 2021).

Analyses of predictability may be more complicated in the tropics, which studies such as Mapes et al. (2008) and Straus and Paolino (2008) suggest may be predictable for beyond two weeks and even up to a month. However, in the tropics, error propagation is presumably set by convection and convectively coupled waves (e.g., Ying & Zhang, 2017), making model studies dependent on the choices involved in the convective parameterization. Another intriguing avenue for future study is the inherent predictability of the stratosphere in different climates.

Data Availability Statement

The Flexible Modeling System may be found at: https://www.gfdl.noaa.gov/fms/ and AM4 is available for download at: https://doi.org/10.5281/zenodo.1199642. SST distributions used to force AM4 are described in the text and illustrated in the Supporting Information.

Acknowledgments
AS thanks Isaac Held for useful communications. This research was supported by the generosity of Eric and Wendy Schmidt by recommendation of the Schmidt Futures program.

References

Daley, R. (1981). Predictability experiments with a baroclinic model. *Atmosphere-Ocean*, *19*, 77–89. https://doi.org/10.1080/07055900.1981.9649102

Eyring, V., Bony, S., Meehl, G. A., Senior, C. A., Stevens, B., Stouffer, R. J., & Taylor, K. E. (2016). Overview of the Coupled Model Intercomparison Project Phase 6 (CMIP6) experimental design and organization. *Geoscientific Model Development*, *9*(5), 1937–1958. https://doi.org/10.5194/gmd-9-1937-2016

Frierson, D. M. W., Held, I. M., & Zurita-Gotor, P. (2006). A gray-radiation aquaplanet moist GCM. Part I: Static stability and eddy scale. *Journal of the Atmospheric Sciences*, *63*, 2548–2566. https://doi.org/10.1175/jas3753.1

Froude, L. S., Bengtsson, L., & Hodges, K. I. (2013). Atmospheric predictability revisited. *Tellus A: Dynamic Meteorology and Oceanography*, *65*(1), 19022. https://doi.org/10.3402/tellusa.v65i0.19022

Harris, L. M., & Lin, S.-J. (2013). A two-way nested global-regional dynamical core on the cubed-sphere grid. *Monthly Weather Review*, *141*, 283–306. https://doi.org/10.1175/mwr-d-11-00201.1

Held, I. M. (1982). On the height of the tropopause and the static stability of the troposphere. *Journal of the Atmospheric Sciences*, *39*, 412–417. https://doi.org/10.1175/1520-0469(1982)039<0412:othott>2.0.co;2

Held, I. M., & Suarez, M. J. (1994). A proposal for the intercomparison of the dynamical cores of atmospheric general circulation models. *Bulletin of the American Meteorological Society*, *75*(10), 1825–1830. https://doi.org/10.1175/1520-0477(1994)075<1825:apftio>2.0.co;2

Judt, F. (2020). Atmospheric predictability of the tropics, middle latitudes, and polar regions explored through global storm-resolving simulations. *Journal of the Atmospheric Sciences*, *77*(1), 257–276. https://doi.org/10.1175/jas-d-19-0116.1

Krishnamurthy, V. (1993). A predictability study of Lorenz's 28-variable model as a dynamical system. *Journal of the Atmospheric Sciences*, *50*, 2215–2229. https://doi.org/10.1175/1520-0469(1993)050<2215:apsolv>2.0.co;2

Liu, H. L., Sassi, F., & Garcia, R. R. (2009). Error growth in a whole atmosphere climate model. *Journal of the Atmospheric Sciences*, *66*(1), 173–186. https://doi.org/10.1175/2008jas2825.1

Lorenz, E. N. (1969). The predictability of a flow which possesses many scales of motion. *Tellus*, *21*, 289–307. https://doi.org/10.3402/tellusa.v21i3.10086

Mapes, B., Tulich, S., Nasuno, T., & Satoh, M. (2008). Predictability aspects of global aqua-planet simulations with explicit convection. *Journal of the Meteorological Society of Japan*, *86A*, 175–185. https://doi.org/10.2151/jmsj.86a.175

Neale, R. B., & Hoskins, B. J. (2000). A standard test for AGCMs including their physical parametrizations: I. The proposal. *Atmospheric Science Letters*, *1*, 101–107. https://doi.org/10.1006/asle.2000.0019

O'Gorman, P. A. (2011). The effective static stability experienced by eddies in a moist atmosphere. *Journal of the Atmospheric Sciences*, *68*(1), 75–90.

Palmer, T. N., Döring, A., & Seregin, G. (2014). The real butterfly effect. *Nonlinearity*, *27*(9), R123. https://doi.org/10.1088/0951-7715/27/9/r123

Polvani, L. M., & Kushner, P. J. (2002). Tropospheric response to stratospheric perturbations in a relatively simple general circulation model. *Geophysical Research Letters*, *29*(7), 1114. https://doi.org/10.1029/2001GL014284

Putman, W. M., & Lin, S.-J. (2007). Finite-volume transport on various cubed-sphere grids. *Journal of Computational Physics*, *227*(1), 55–78. https://doi.org/10.1016/j.jcp.2007.07.022

Sheshadri, A., & Plumb, R. A. (2016). Sensitivity of the surface responses of an idealized AGCM to the timing of imposed ozone depletion-like polar stratospheric cooling. *Geophysical Research Letters*, *43*, 2330–2336. https://doi.org/10.1002/2016GL067964

Sheshadri, A., Plumb, R. A., & Gerber, E. P. (2015). Seasonal variability of the polar stratospheric vortex in an idealized AGCM with varying tropospheric wave forcing. *Journal of the Atmospheric Sciences*, *72*(6), 2248–2266. https://doi.org/10.1175/jas-d-14-0191.1

Simmonds, I., & Li, M. (2021). Trends and variability in polar sea ice, global atmospheric circulations, and baroclinicity. *Annals of the New York Academy of Sciences*, *1504*, 167–186. https://doi.org/10.1111/nyas.14673

Smagorinsky, J. (1969). Problems and promises of deterministic extended range forecasting. *Bulletin of the American Meteorological Society*, *50*(5), 286–312. https://doi.org/10.1175/1520-0477-50.5.286

Stone, P. H. (1978). Baroclinic adjustment. *Journal of the Atmospheric Sciences*, *35*, 561–571. https://doi.org/10.1175/1520-0469(1978)035<0561:ba>2.0.co;2

Straus, D. M., & Paolino, D. (2008). Intermediate time error growth and predictability: Tropics versus mid-latitudes. *Tellus*, *61*, 579–586. https://doi.org/10.1111/j.1600-0870.2009.00411.x

Sun, Y. Q., & Zhang, F. (2016). Intrinsic versus practical limits of atmospheric predictability and the significance of the butterfly effect. *Journal of the Atmospheric Sciences*, *73*(3), 1419–1438. https://doi.org/10.1175/jas-d-15-0142.1

Ying, Y., & Zhang, F. (2017). Practical and intrinsic predictability of multiscale weather and convectively coupled equatorial waves during the active phase of an MJO. *Journal of the Atmospheric Sciences*, *74*, 3771–3785. https://doi.org/10.1175/jas-d-17-0157.1

Zhao, M., Golaz, J. C., Held, I. M., Guo, H., Balaji, V., Benson, R., et al. (2018a). The GFDL global atmosphere and land model AM4.0/LM4.0: 1. Simulation characteristics with prescribed SSTs. *Journal of Advances in Modeling Earth Systems*, *10*, 691–734. https://doi.org/10.1002/2017MS001208

Zhao, M., Golaz, J. C., Held, I. M., Guo, H., Balaji, V., Benson, R., et al. (2018b). The GFDL global atmosphere and land model AM4.0/LM4.0: 2. Model description, sensitivity studies, and tuning strategies. *Journal of Advances in Modeling Earth Systems*, *10*, 735–769. https://doi.org/10.1002/2017MS001209